This is a repository copy of *A columnar liquid quasicrystal with a honeycomb structure that consists of triangular, square and trapezoidal cells*.

Article:

A Columnar Liquid Quasicrystal with a Honeycomb Structure that Consists of Triangular, Square and Trapezoidal Cells

Xiangbing Zeng[1], Benjamin Glettner[2], Ute Baumeister[2], Bin Chen[2], Goran Ungar[1,3], Feng Liu[3], & Carsten Tschierske[2]

[1]Department of Materials Science and Engineering, Sheffield University, Sheffield S1 3JD, UK.

[2]Institute of Chemistry, Martin Luther University Halle-Wittenberg, Kurt-Mothes-Strasse 2, Halle/Saale D-06120, Germany.

[3]State Key Laboratory for Mechanical Behaviour of Materials, Shaan-xi International Research Centre for Soft Matter, Xi'an Jiaotong University, Xi'an, 710049, P. R. China.

Corresponding author: Xiangbing Zeng, x.zeng@shef.ac.uk

Quasicrystals are intriguing structures, having long-range positional correlations but no periodicity in parallel (i.e. real) space, typically with rotational symmetries that are "forbidden" in conventional periodic crystals. Here we present a two-dimensional columnar liquid quasicrystal with dodecagonal symmetry. Unlike previous dodecagonal quasicrystals based on random tiling, a honeycomb structure based on strictly quasiperiodic tessellation of tiles is shown to be possible. The structure consists of dodecagonal clusters made up of triangular, square and trapezoidal cells that are optimal for local packing. To maximize the presence of such dodecagonal clusters, the system abandons periodicity but adopts a quasiperiodic structure following strict packing rules. The stability of random-tiling dodecagonal quasicrystals is often attributed to the entropy of disordering when strict tiling rules are broken, at the sacrifice of the long-range positional order. However, our results demonstrate that quasicrystal stability may rest on energy minimization alone, or with only minimal entropic intervention.

The discovery of quasicrystals[1] in metal alloys in 1984 - for which Prof. Shechtman would be awarded the Nobel prize in chemistry in 2011 - changed our preconception that any structure with long range positional order must be periodic[2]. While a common crystal can be described as a periodic repetition of a single unit cell, a quasicrystal has multiple building blocks (tiles) of different shape. Such tiles pack locally into clusters with a symmetry such as pentagonal or dodecagonal, which is forbidden in classical crystallography and is incompatible with a real (parallel) space periodic lattice. To make such symmetry global while keeping the long-range positional order (quasicrystals diffract like normal periodic crystals), strict and often complex tiling rules must be followed, as in the famous Penrose "kite and dart" tiling (Fig. **1a**)[3,4].

The first liquid quasicrystal (LQC) was discovered in 2004,[5] formed by dendritic molecules self-assembled into spherical micelles on a dodecagonal quasiperiodic lattice. This was analogous to atomic packing in metallic dodecagonal quasicrystals,[6,7] but at the nano-meter scale instead of atomic scale, i.e. Angstroms. Since then more nano- and meso-scale quasicrystals were found in other soft and hard synthetic systems[8,9,10,11,12,13,14,15]. The unusual combination of long-range positional order and high rotational symmetry

(invariant under a combination of rotational and translational operations) makes nanoscale quasicrystals interesting for applications e.g. in wide band-gap photonics.[16] The universality of quasicrystal structures across length scales has also attracted much theoretical interest[17,18,19,20].
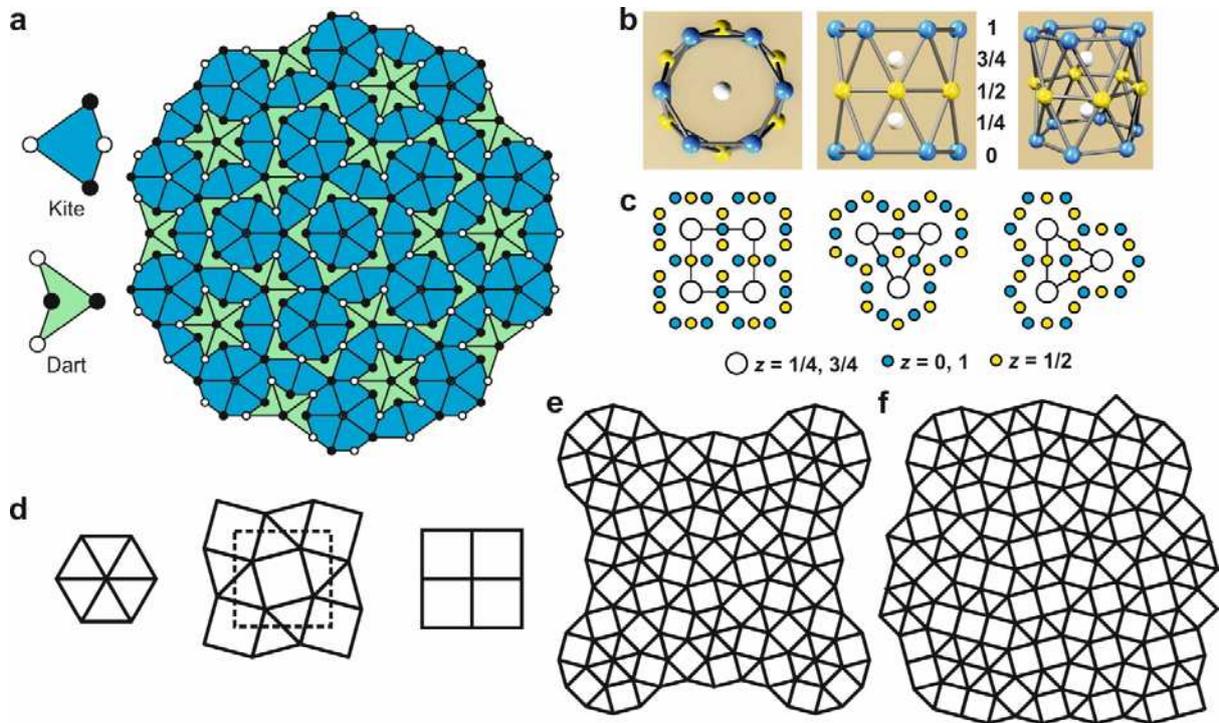

Fig. 1. Quasiperiodic tilings and their differences to normal periodic tilings. **a**, Penrose "Kite and Dart" tiling. The vertices of the tiles are marked with empty and solid circles, which must be matched (tiling rule) to create the quasiperiodic tiling with 5-fold rotational symmetry[4]. The tiling never repeats itself completely on simple translations. **b**, A local tetrahedral close packed cluster of spheres, consisting of two hexagonal antiprisms, with $\overline{12}$ symmetry[5]. Left: top view, Middle: front view, Right: 3D view. **c**, Arrangement of the hexagonal antiprisms (as shown in **b** with slight distortion) on square and triangular tiles. **d**, Examples of periodic tilings using triangles and squares, that can be generated by periodic translation/repetition of two triangles (Left), a square (Right), and a particular combination of triangles and squares (Middle) that can be viewed as a larger decorated square tile as outlined by the meshed lines. **e**, A quasiperiodic dodecagonal tiling of squares and triangles[22]. It follows a set of strict tiling rules and is invariant only under certain combinations of rotational and translational operations. **f**, An example of random tilings of squares and triangles[23]. It can be viewed as a dodecagonal quasiperiodic tiling but with many "defects" where strict tiling rules are not observed.

The origin of quasicrystalline structures in the packing of soft spheres, such as spherical dendron assemblies and metal atoms, is linked to the fact that locally four identical spheres pack most efficiently by forming a regular tetrahedron. However, regular tetrahedra cannot fill space without leaving gaps. In metallic alloys, and later in their soft matter counterparts, this leads to the formation of a series of phases with complex (either periodic or quasiperiodic) structures, where spheres form only tetrahedral interstices but with

distortions. Such phases were first classified by Frank and Kasper hence the name Frank-Kasper (F-K) phases[21]. In F-K phases the coordination number of an atom (or a soft sphere) can be either 12, 14, 15 or 16, hence different environment at different sites that can be accommodated by different atomic species in alloys, or the deformation of soft spheres. A common local packing of soft spheres in F-K phases takes the form of a hexagonal antiprism with $\overline{12}$ symmetry (Fig. 1**b**). Such antiprisms can be arranged to form squares or triangles (Fig. 1**c**), and tilings of the plane by such squares and triangles in turn produce a number of different periodic (Fig. 1**d**) and quasiperiodic (Fig.1**e**) structures. While the rules for dodecagonal square-triangle quasiperiodic tiling are complex[22], a random tiling of squares and triangles[23] (Fig. 1**f**), without any tiling rules, is always observed experimentally[24]. The randomness of the tiling reduces the long-range positional order, as breaking of the tiling rules leads to local periodic patches (phason defects). However, such randomness increases the entropy of the phase and is considered to contribute to its stability.

In metal alloys a variety of different quasicrystals are observed, owing to the range of atom sizes and compositions available. However, in the nano- and meso-scale quasicrystals realized so far, the variety is very limited. In fact most of them are dodecagonal and based on random square-triangle tiling[8-15]. Patchy colloidal tiles have been artificially fabricated and assembled into a 2D quasicrystal following strict tiling rules, where the tiles were attached to a glass surface through a thin water soluble coating. However, once the structure was "released", on the addition of an aqueous solution that dissolved the coating, the strict quasicrystalline order could no longer be maintained, as Brownian motion led to fluctuations and worsening of quasicrystalline order[25]. Similarly, a numerical study of pentagonal platelets suspended in a nematic liquid crystal suggested the formation of quasicrystal[26], but experimentally only small patches of such a structure have been realized[27]. For model star-like tiles based on DNA origami particles the stabilization of quasicrystals by local directional bonding has recently been proposed based on simulation[28,29].

In this work we show experimentally, by using self-assembled molecular tiles with a degree of flexibility, how a 2D nanoscale quasicrystal can be obtained with true quasiperiodic order based on strict tiling rules.

Results

Compound and phase sequence

The compound we studied is a T-shaped molecule (compound **1**), consisting of a rigid rod-like aromatic (*p*-terphenyl) core, two alkyl end-chains and a polar ionic group attached to an oligoethylene oxide lateral chain (Fig. 2**a**). Due to the tendency of the three incompatible but connected parts to nanophase separate, such T-shaped polyphiles are extremely versatile in forming different 1D, 2D and 3D liquid crystal (LC) structures.[30,31] Compound **1** displays several phases of "honeycomb" type (Fig. 2**b**). These consist of

3

"inverse" columns with a range of polygonal cross-sections (Figs. 2**c, e**).[32] The rigid molecular cores form the flat side walls of the prismatic cells, their end-groups aggregating at cell edges and the lateral chains occupying the interior of the cells.

All previously discovered liquid crystalline phases formed by T-shaped molecules with long range positional order, including all the honeycomb phases, are periodic. This is despite the fact that it has long been speculated that a quasicrystalline phase might be observed in the tiling region between triangles and squares, as most soft quasicrystals are. Notably, there is a big jump (by >73%) in the volume-to-surface area ratio upon going from a triangular to a square column, and a phase consisting of two square and four triangular columns ("snub-square" tiling) in the unit cell with plane group *p4gm* has been found previously (Fig. 2**e(ii)**).[31,32] It is also interesting to note that in the *p4gm* phase, the molecular backbones at a square-triangle boundary shift towards the square (shown by arrows in Fig. 2**e(ii)**). Hence square columns shrink and triangular ones expands in order to balance their volume-to-surface area ratios, a fact that we will return to later.

Four different LC phases have been observed in compound **1** at different temperatures (Fig. 2**b**). The phase transitions are induced by the change of the ratio between the lateral chain volume and molecular length, the former expanding with increasing temperature and the latter contracting. Two of the phases have been discovered previously in other T-shaped compounds and their structures are well understood. They are the triangular columnar phase (Col$_{hex}\Delta$)[31,33], with plane group *p6mm*, found at temperatures below 60°C (Fig. 2**c**), and the 3D hexagonal phase (3D-Hex, Fig. 2**d**),[34] with space group *P*6/*mmm*, between 80°C and the isotropization temperature at 88°C. For their lattice parameters and reconstructed electron density maps see Supplementary Tables 1,5 and Figs. 7,11.
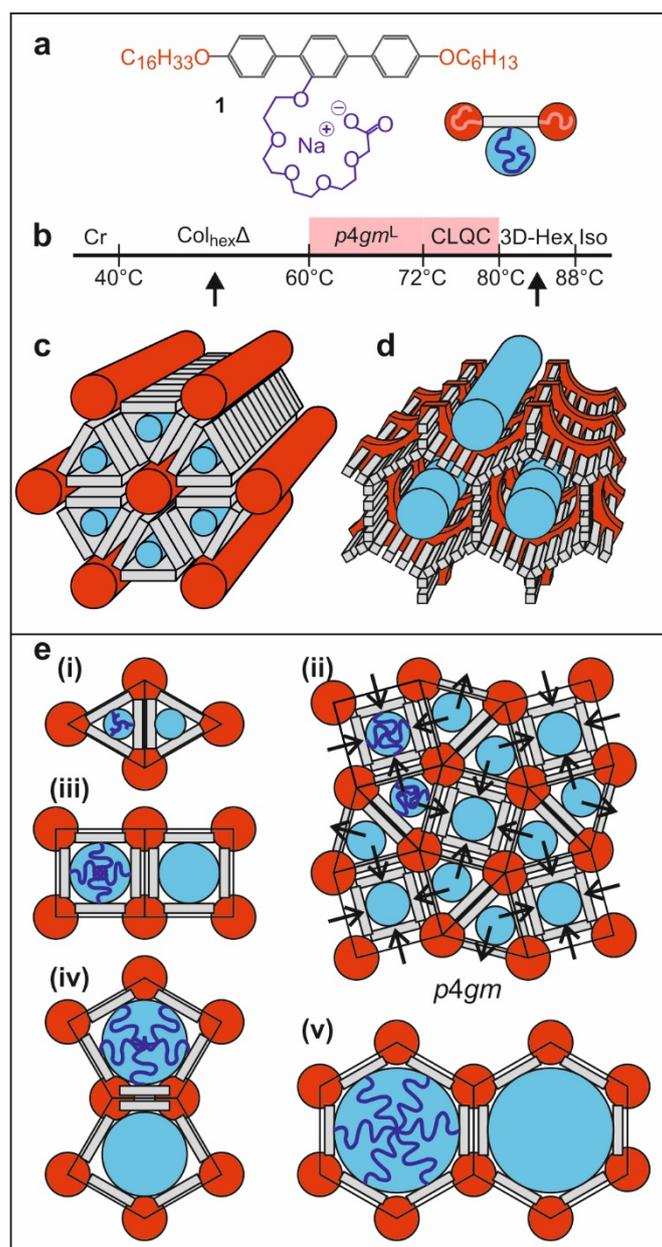
Fig. 2. T-shaped polyphilic molecules and their self-assembly. **a**, Compound **1** under present study is a T-shaped polyphile, with a terphenyl backbone (coloured in grey), two alkyl end chains (red) and a polar side group (blue). **b**, Phase sequence of compound **1** on heating. Four different liquid crystalline phases are observed, with two new phases that will be the main focus of the current study highlighted in pink. **c**, In the $Col_{hex}\Delta$ phase of compound **1** observed between 40°C and 60°C, T-shaped molecules self-assemble into a honeycomb columnar phase with triangular cells. **d**, In the 3D-Hex phase of compound **1** observed between 80°C and 88°C, lamellae of alternating backbones and end chains of molecules are penetrated by a hexagonal array of columns of their side groups. **e**, Schematic drawings showing how T-shaped molecules form "honeycomb" phases of "inverse" columns with polygonal cross-sections, from (**i**) triangles, (**ii**) combination of squares and triangles, (**iii**) squares, (**iv**) pentagons to (**v**) hexagons with increasing side group volume. Previously discovered $p4gm$ phase (**ii**)[31,32] consists of mixed triangular and square columns (4-fold rotational axes at the centres of squares, glide planes along the sides, and mirror planes

5

along the diagonal of the unit cell). Note the expansion of the triangular columns and the shrinkage of the square ones in (**ii**), as indicated by arrows at the boundaries between square and triangular cells. This is to equalize the density of the side groups since in undistorted square and triangular columns, as shown in (**iii**) and (**i**) respectively, the area per chain would be 1/4= 0.25 and $\sqrt{3}/12$ = 0.144, a difference by >73%.

X-ray diffraction studies on powder and oriented samples

The other two phases are new and are observed in compound **1** in the temperature range between the Col$_{hex}\Delta$ and the 3D-Hex phases. The powder diffractograms of the two phases, recorded at 70°C and 75°C respectively, are displayed in Fig. 3**a**. The diffraction peaks of the 70°C phase can be indexed on a square lattice with lattice parameter a = 16.7 nm, with calculated d-spacings of diffraction peaks almost the same as those experimentally observed (with error <0.01 nm, details see Supplementary Table 2 and Figs. 8,9). The plane group of the phase is determined as *p4gm*, since the only observed extinction rule is that no (h0) peak with h odd, (10), (30), (50) etc., was observed. This phase will be referred to here as *p4gm*^{L}, with L for large, as its unit cell is larger and different from that of the previously known *p4gm* phase of mixed triangles and squares (Fig. 2**e**(**ii**)). $a_{p4gm}{}^L$ is about twice that of a_{p4gm}, and (41) and (33) are the dominant reflections of *p4gm*^{L} instead of the (20) and (21) in the *p4gm*.

The diffractogram collected at 75°C looks very similar to that at 70°C but with significantly fewer split peaks. For example, the dominant (41) and (33) peaks of the *p4gm*^{L} phase have now merged into a single peak. The polarized microscopy texture hardly changes at the transition between the two phases, suggesting their strong structural similarity (Supplementary Fig. 5). However, no satisfactory indexing of the diffraction peaks using a 2D or 3D periodic lattice could be achieved. Instead, it was found that the q^2 ratio of the first four observed peaks are 1:2:3:3.72, very similar to the expected q^2 ratio of 1:2:3:3.732 (1:2:3:2 $+ \sqrt{3}$) between (1000), (1001), (1010) and (1100) peaks of a 2D quasicrystal with 12-fold rotational symmetry, with four instead of two reciprocal lattice basis vectors. Indeed, assuming a 2D dodecagonal quasiperiodic lattice, all the observed diffraction peaks could be indexed with only a <1% error between experimental and calculated *d*-spacings (Table S3). This **C**olumnar **L**iquid **Q**uasi**C**rystalline phase is referred to as CLQC hereafter.

That this high temperature phase is indeed dodecagonal, hence quasiperiodic, is further confirmed by the 12-fold rotational symmetry of its grazing-incidence X-ray diffraction (GIXRD) pattern (Fig. 3**b**) recorded from a surface-oriented thin film. The CLQC domains in the film are all oriented with one of their twelve equivalent {1100} reciprocal lattice vectors perpendicular to the substrate surface. Such surface directed orientation is commonly observed in honeycomb phases formed by T- and X-shaped molecules, and in the current case to maximize the contact of the hydrophilic side groups with the also hydrophilic silicon surface.[35] The diffraction pattern is therefore equivalent to that from a single CLQC crystal rotating around its vertical (0110) axis. Due to the geometric limitation of GIXRD, only the upper half of the *q*-space is visible. However, the strongest {1100} peaks are still visible below the horizon, with their intensities greatly reduced due to absorption in the

substrate. In Fig. 3**b** the dodecagonal reciprocal lattice is overlaid on the GIXRD pattern, clearly showing the 12-fold rotational symmetry and the coincidence of experimental spots and the theoretical lattice nodes. The integrated intensities of diffraction peaks of the same reflection group are also the same within experimental error after correction for experimental geometry (Supplementary Table 3). The diffraction peaks of the CLQC are as sharp as observed for the $p4gm^L$ (Supplementary Fig. 12) and other liquid crystalline phases of compound **1**, with a domain size of $>0.4\mu m$ estimated from the measured peak width. GISAXS experiments on oriented samples are able to discern very finely split diffraction peaks, as well as small differences in system symmetry. An example of this is shown in supplementary Fig. 9, where the discrimination of closely spaced peaks of the $p4gm^L$ phase leads to a perfect match between experiment and model. Furthermore, given the high experimental resolution, we can state with confidence that there is very little anisotropic broadening or distortion of the diffraction peaks of CLQC, suggesting low concentration of phasonic defects and a true quasiperiodic order. The low concentration of phason defects is also supported by the observation that diffraction peak width increases with increasing diffraction angle (i.e. q-value in the real space) in CLQC, same as in periodic $p4gm^L$ (Supplementary Fig. 13a), but has no correlation to its q-value in the perpendicular space (Supplementary Fig. 13b).
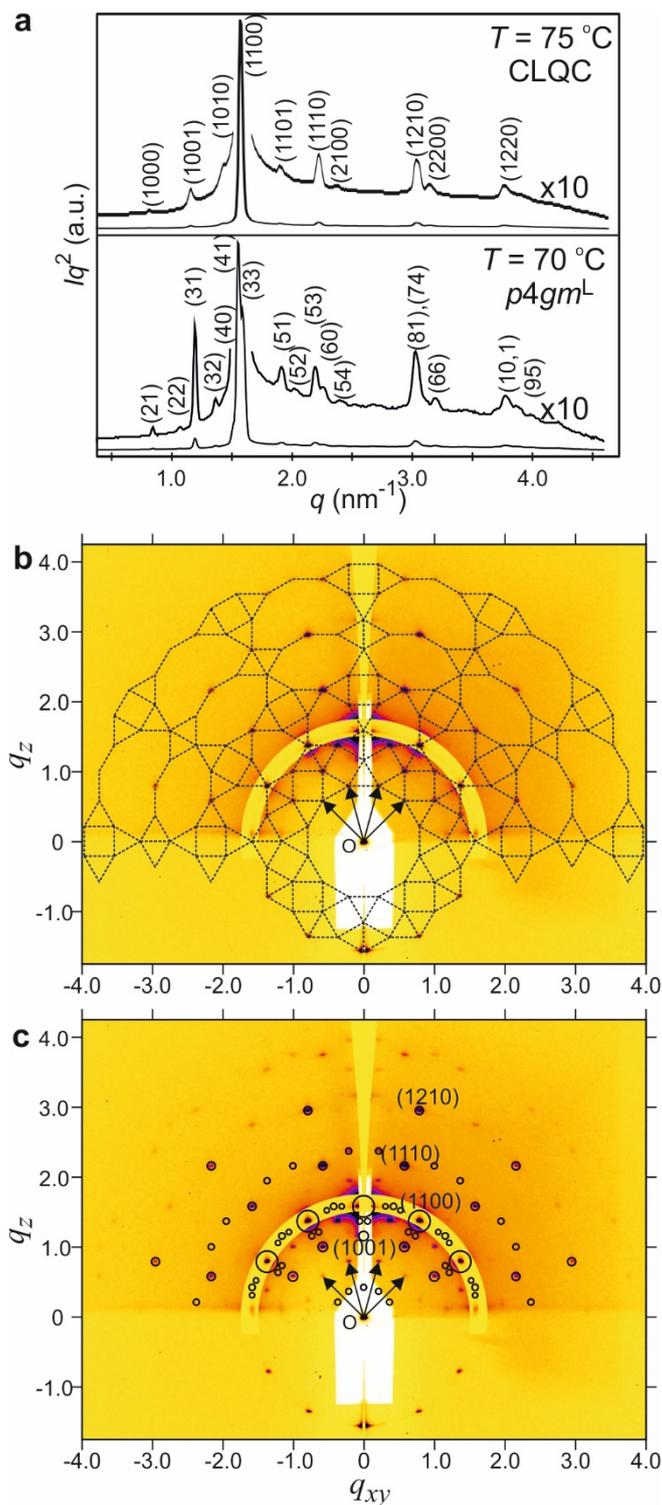
Fig. 3. X-ray diffractograms of the CLQC and $p4gm^L$ phases of compound **1**. **a**, Indexed powder X-ray diffractograms of CLQC and $p4gm^L$ phase, collected at 75°C and 70°C respectively. GIXRD pattern of the CLQC phase of compound **1**. **b**, The GIXRD pattern of CLQC recorded at 75°C and mapped into the q-space, with reciprocal lattice overlaid on top. As the {1100} reflections are much stronger than the rest, their intensities on a narrow band around the peaks are scaled down 100 times. **c**, Comparison of experimental and simulated diffraction patterns. Only peaks with intensities higher than 0.5% of that of the (1100) are shown in the simulated pattern, where each peak is represented by a circle, the

area of which is proportional to the absolute value of the calculated amplitude of the peak, or the square root of the peak intensity.

Electron Density Maps and Structural Models

In order to understand the structure of the CLQC, we first examine the structure of the $p4gm^L$ phase. On the basis of the assigned plane group and measured diffraction intensities, the electron density map of the phase has been reconstructed (for details see Methods) and shown in Fig. 4**a**. In the map the red low electron density regions correspond to the aliphatic end-chains, and the blue high electron density regions to the polar side-chains. Having identified such regions in the map, the framework of the honeycomb columnar structure has been constructed and overlaid on the map. In addition to triangular and square-shaped columns, a third kind of columns, trapezoidal in cross-section, can be identified. It is also the case that four such trapezoidal columns and two square columns always join together and form an octagon (outlined in yellow in Fig. 4**a**). The six columns of the octagon share a common vertex of aliphatic end groups which is elliptical rather than circular as in other vertices shared by only five columns. The stretched vertex makes up the fourth side of the trapezoid, while the other three sides are the rigid aromatic walls. It should be noted that a periodic honeycomb composed of only trapezoidal columns has been reported previously.[36]

While the electron density map of the CLQC phase is non-trivial to reconstruct[37,38] due to its lack of periodicity, we have examined instead an imaginary approximant of CLQC with an e**x**tra-**l**arge square unit cell (a = 32.1 nm), also plane group $p4gm$ (named $p4gm^{XL}$). Here e.g. the twelve {1100} diffraction spots of CLQC are mapped onto the four {80} plus eight {74} peaks of the approximant (Supplementary Table 4). It should be stressed that the resolution of our experimental setup is able to distinguish the diffraction pattern of an approximant, with unit cell dimension as large of 100 nm, from that of the quasicrystal with perfect 12-fold symmetry. The electron density map of the approximant, has subsequently been reconstructed using the intensities of the corresponding CLQC peaks and shown in Fig. 4**b**. The same kind of triangular, square and trapezoidal columns are observed as in the $p4gm^L$ phase. Four trapezoidal and two square columns again always join together to form an octagon. A dodecagon, consisting of four triangles, one square and two octagons, is the basic tile that has been used to generate the periodic tiling of the plane in the $p4gm^{XL}$ phase. Molecular arrangement in the dodecagon is schematically shown in Fig. 4**c**. Like in the small-cell $p4gm$ phase (Fig. 2**e**(**ii**)), the square columns shrink and the triangular ones expand.
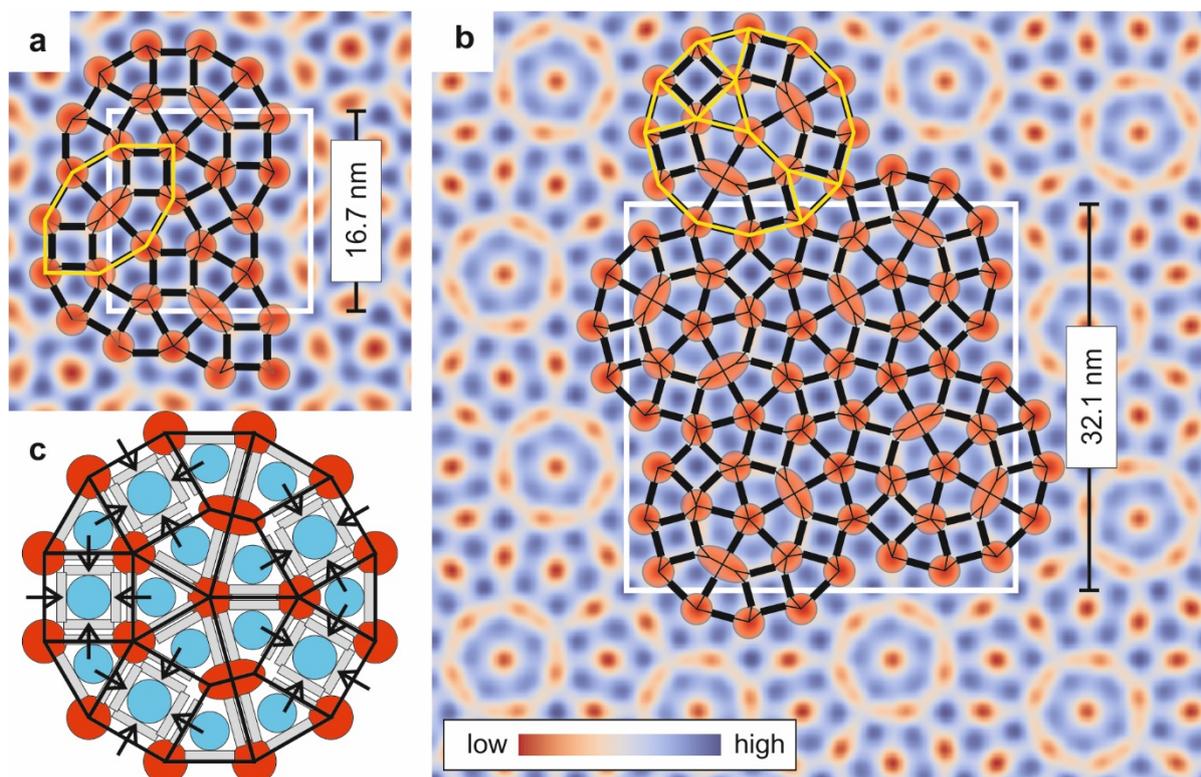
Fig. 4. Reconstructed electron density maps. **a**, Reconstructed electron density map of the *p4gm*[L] phase, the unit cell is shown in white lines. Schematic outlines of the polygonal columns that form the phase are overlaid on the map, with semi-transparent circles and ellipses representing the soft corners of aliphatic end-groups (low electron density regions, red in the map), and thick black lines representing the rigid molecular cores (medium electron density, white in the map). The high electron density polar side groups are blue in the map. Triangular, square and trapezoidal columns can be identified. Yellow lines outline an octagon formed by four trapezoidal and two square columns that share an elliptically distorted aliphatic vertex at the centre. **b**, Reconstructed electron density map of an imaginary approximant of CLQC with *p4gm* symmetry (*p4gm*[XL]); the four {80} and eight {74} diffraction peaks of the approximant would merge into the twelve {1100} peaks of the CLQC. The same triangular, square and trapezoidal columns, as found in (**a**), can be identified. Here the yellow lines outline a recurring dodecagon, consisting of four triangles, a square, and two octagons. **c**, Schematic drawings of molecular arrangement in the dodecagon, with shrinking of the square columns and expansion of the triangular columns indicated by arrows.

The same dodecagon can be used to tile a plane quasiperiodically. Such tilings can be generated using the fact that a periodic dodecagonal lattice, while impossible in 2D or 3D, does exist in 4D. Projection of all the 4D lattice points into the 2D space will effectively fill the whole plane, but a dodecagonal quasiperiodic lattice will be generated if only a suitable selection of the lattice points in 4D are projected[39]. Each of these 4D lattice point vector, is a combination of two vectors. The first one is its projection into the 2D real space (or parallel space), the other is its projection into an imaginary 2D space (or perpendicular space as it is perpendicular to the real space). The selection rule can be implemented by

defining an "acceptance domain" in the perpendicular space, that a particular lattice point is only selected when its projection in the perpendicular space is inside the domain (cut-and-project method, Supplementary S2.1)[39]. Fig. 5**a** shows the acceptance domain in the shape of three overlapping squares (coloured in blue), that generates a quasiperiodic tiling on the basis of the dodecagon, which consists of four triangles, one square and two octagons (Figs. 4**b,c** and 5**b**). Increasing the size of the acceptance domain to include the pink regions in Fig. 5**a**, two extra lattice points will be introduced inside each octagon and the basic tiles become triangles, squares and thin rhombi (Fig. 5**b**). The decoration of the dodecagon as four triangles, five squares and eight trapezoids is shown in Fig. 5**c**. This can be translated into the corresponding honeycomb structure as schematically drawn in Fig. 5**d**, with the expected electron density map shown in Fig. 5**e**. The dodecagonal symmetry and the quasiperiodic nature of the lattice generated by the blue acceptance domain in Fig. 5**a** are shown in larger areas in Figs. 5**f,g**.

On the basis of this dodecagonal quasiperiodic lattice, we are able to simulate the diffraction pattern of CLQC by decorating each lattice point with a cylindrical function $f(r)$. $f(r)$ has an electron density minimum at $r = 0$ (representing the aliphatic chains at the corners of the columns), and a maximum at $r = \rho\, a_{//}$, representing the high electron density polar groups which tend to accumulate at the centres of the tiles at a particular distance $\rho\, a_{//}$ from the corners (Fig. 5**h**, bottom). Taking the distribution widths of the positive and negative peaks, and the ρ-value as the three fitting parameters, a reasonable fit to the experimentally observed diffraction intensities has been achieved, as presented in Supplementary Table S3. The fit is also shown graphically in Fig. 3**c** by overlaying circles of area proportional to calculated diffraction amplitude on the corresponding experimental GIXRD spots. The decoration procedure also takes into account the fact that the number of molecules connected to each pink lattice point is only 60% of that connected to each blue lattice point. For details of the simulation see Supplementary S2.3. The simulated ("decorated") electron density map of a dodecagon is shown in Fig. 5**h** for easier visual comparison with the reconstructed ED maps in Figs. 4**a,b**. Though our current structural model of CLQC is not the only one compatible with the observed X-ray diffraction data, the tiling motif corresponds to the approximant $p4gm^{L}$ phase, and in addition, it is fully consistent with the molecular dimensions.
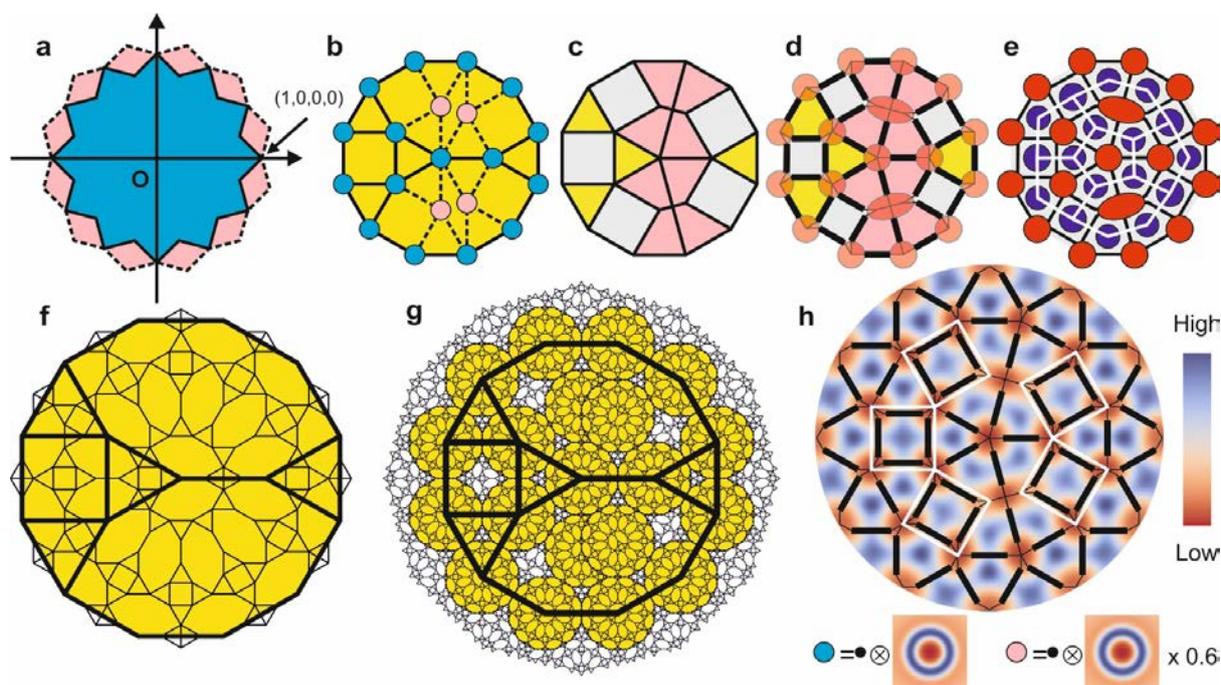
Fig. 5. Model of CLQC on the basis of a quasiperiodic tiling of plane using triangles, squares and trapezoids. **a**, The acceptance domain in perpendicular space, blue for the triangle-square-octagon tiling. **b**, The dodecagon unit generated using the acceptance domain. The addition of pink regions leads to two extra (pink) lattice points inside each octagon, breaking the octagon into two squares, four triangles and one thin rhombus. **c**. Decoration of the dodecagon tile as four triangles, five squares and eight trapezoids. **d**, The schematic framework showing how molecules arrange in the dodecagonal tile. **e**, Schematic electron density map, red: low density aliphatic regions, blue: high density polar regions, grey: medium density rigid aromatic cores. White lines connecting the centres of the high density polar regions show the dual tiling of the dodecagon by distorted pentagons and hexagons. **f, g**, Larger patches of the quasiperiodic tiling generated by the cut-and-project method (Supplementary S2). **h**, A simulated electron density map is generated numerically by convolution of each lattice point with a radial distribution of electron density (bottom of panel **h**) that has a minimum at centre, and a maximum at distance about 60% of the distance between neighbouring lattice points (Supplementary S2). The map is very similar to that of reconstructed ones in Fig. 4, consisting of triangular, square and trapezoidal columns where low electron density aliphatic chain regions are in red, medium electron density rigid cores white, and high electron density polar groups blue. It also supports that rigid terphenyl cores (represented by thick black lines) along the sides of the square columns shift inwards, as highlighted by the original undistorted square tiles (white lines) overlaid on top.

A feature clearly visible in the experimentally reconstructed (Figs. 4**a**,**b**) and simulated (Fig. 5**h**) ED maps is that in the square cells the rigid terphenyl cores along the sides shift inwards, as highlighted in Fig. 5**h** and shown in Fig. 6**a**. As mentioned previously regarding the *p4gm* phase (Fig. 2**e(ii)**), such polygon shrinkage helps balance the volume/surface-area ratio for columns of different shape, enabling the triangular and trapezoidal columns to expand into the space of neighbouring squares and distributing the packing density more

12

uniformly. This helps to explain why, unlike in micellar dodecagonal quasicrystals[24,40], in this quasiperiodic tiling a square tile never shares a common edge with another square tile, and why a triangular tile only has up to one triangular neighbour. Similar rules also apply to the octagons and dodecagons, e.g. they never share a square edge (coloured red in Fig. 6**b**) with another octagon or dodecagon.

In fact the stability of CLQC over periodic alternatives can be explained by the drive to maximize the coverage of the plane by dodecagons, locally the most stable entities, while abiding by the tiling rules prescribed by their coloured edges (Figs. 6**b,c**). As each dodecagon has only seven blue (non-square) edges, it can have only up to seven nearest dodecagonal neighbours. Among the seven, two pairs must overlap and share an octagon, and their orientations are therefore fixed (Fig. 6**d**). This adds further restrictions to how the other three dodecagons should orient. The result is a larger dodecagon (Fig. 6**e**) with its edge length inflated by a factor of $2 + \sqrt{3}$ compared to the original. The inflated dodecagon also consists of four triangles, one square and two octagons, all equally inflated. It also has coloured edges and obeys the same tiling rules (Figs. 6**f,g**). In fact, the same quasiperiodic tiling of the plane by triangles, squares and octagons as produced by the cut-and-project method (Supplementary S2.1), can be generated by such repeated inflation/decoration steps. The tiling by dodecagons in Fig. 6**e** is exactly the same as shown in Fig. 5**f**, and a further inflation step leads to a still larger dodecagon and the patch shown in Fig. 5**g**.
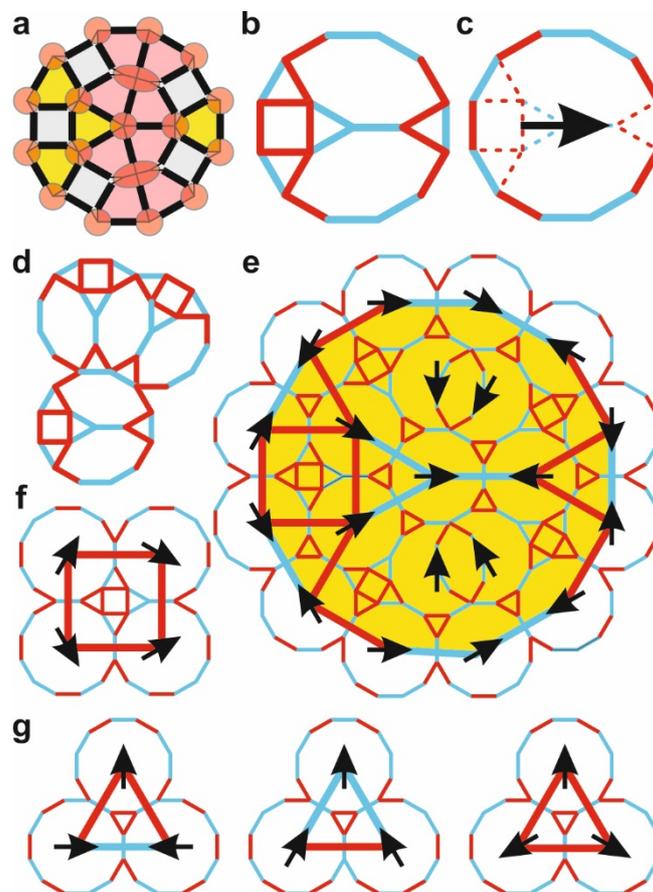
Fig. 6. Tiling and inflation rules that leads to the dodecagonal quasiperiodic tiling of CLQC. **a**. A dodecagon, consisting of shrunk square and expanded triangular columns. **b**. A dodecagon consisting of four triangles, one square and two octagons, has five of its twelve outer edges coloured red (square edges) that cannot be shared with another dodecagon, leading to complex tiling rules. **c**. The arrangement of the red outer edges can be indicated by an arrow in the centre of the dodecagon. **d**. Two overlapping dodecagons, sharing an octagon, can attach to another dodecagon by their two neighbouring blue sides. **e**. Each dodecagon can be surrounded by up to seven nearest neighbours, locally the densest possible tiling of dodecagons, leading to an inflated dodecagon upon which the same tiling rules apply. **f**, Inflation rules for squares, and **g**, for triangles.

Discussion

It is interesting that the strict tiling rules of the current quasiperiodic tiling can be directly attributed to improved packing efficiency and density uniformity. This is in contrast to many previously found dodecagonal quasicrystals, where the high entropy of a "random" triangle-square tiling due to phason fluctuations is often considered responsible for the phase stability, and as supported by STM images of surface layers,[41] AFM images of micellar LQC phase[24], and TEM images of quasicrystals in star-copolymers[8] and mesoporous silica[12].

It is also worth mentioning that the fact that the most prevalent quasiperiodic structure observed in soft matter is dodecagonal has often been attributed to the soft pair-wise potentials between spherical particles.[42] However, in T-shaped molecules restrictions imposed by the molecular shape play a much more important role.

It is expected that more examples of CLQCs will be found in other T-shaped molecules with different combinations of end- and side-groups, with backbones of different type and length, particularly that might promote semiconducting and optical properties for different applications. [30,31,43] We expect that by fine tuning of the molecular parameters the temperature range of the CLQC phase could be stretched to room temperature if potential applications require it. This may include preparation of eutectic mixtures, a standard route in bringing LC properties to ambient temperature. The self-assembly of the T-shaped molecules into polygonal shaped tiles, and intricate tiling rules resulting from geometric interactions between such tiles in CLQC, suggest that other 2D and 3D LQCs with polygonal or polyhedral shaped tiles could be designed in a similar way. This may possibly lead to e.g. a 2D pentagonal LQC with the famous Penrose tiling[3], as well as icosahedral quasicrystal (IQC) which has been reported in computational studies[29,44] but not yet observed experimentally so far in soft matter.

X-shaped molecules with two instead of one lateral chain have also been found to form honeycomb columnar structures in a similar way to T-shaped molecules.[45] In addition, the two lateral chains can be chemically incompatible as well, adding to the complexity of the honeycomb phases, leading to multi-colour and multi-shape tilings.[46,47] A dual structure of the current CLQC, with pentagonal and hexagonal columns, is also possible (Fig. 5**e**, white

lines). We believe it is only a matter of time before more CLQCs and LQCs of different symmetries are found in T- and X-shaped compounds, and potentially even multi-coloured LQCs in the latter.

Conclusion

The first columnar liquid quasicrystal has been discovered in a T-shaped amphiphilic compound. Having dodecagonal symmetry, its structure has been determined to consist of triangular, square and trapezoidal columns, creating a unique quasiperiodic tiling of the plane. We have shown that the driving force for quasiperiodicity in this new CLQC could be attributed primarily to optimization of packing, i.e. lowering of the system energy rather than increasing the randomness/entropy as in the case of previously found soft quasicrystals. This opens an approach to creating other strict instead of random quasiperiodic structures in soft matter.

Author contributions C.T. and G.U. conceived and directed the project. B.G., U.B., B.C., under the supervision of C.T., synthesized the compound and carried out the DSC, POM and initial XRD characterizations. X.Z. and F.L., supervised by G.U., carried out the powder and GIXRD experiments, and data analysis leading to reconstruction of electron density maps. All authors contributed to the construction of the structural model of the CLQC phase. Simulation of CLQC diffraction pattern was carried out by X.Z. X.Z. wrote the manuscript with written contributions from all co-authors.

Competing interests The authors declare no competing interests.

References

1. Shechtman, D., Blech, I., Gratias, D. & Cahn, J.W. Metallic Phase with Long-Range Orientational Order and No Translational Symmetry. *Phys. Rev. Lett.* **53**, 1951-1953 (1984).
2. Steurer, W. & Deloudi, S. *Crystallography of quasicrystals. Concepts, Methods and Structures*. Springer-Verlag, London, 2009.
3. Penrose, R. The role of aesthetics in pure and applied mathematical research. *Bull. Inst. Math. & its Applns.* **10**, 266-271 (1974).
4. Senechal, M. *Quasicrystals and geometry*, Cambridge University Press (1996).
5. Zeng, X.B., Ungar, G., Liu, Y.S., Percec, V., Dulcey, A.E. & Hobbs, J.K. Supramolecular dendritic liquid quasicrystals. *Nature* **428**, 157-160 (2004).
6. Ishimasa, T., Nissen, H.-U. & Fukano, Y. New ordered state between crystalline and amorphous in Ni-Cr particles. *Phys. Rev. Lett.* **55**, 511–513 (1985).
7. Chen, H., Li, D. X. & Kuo, K. H. New type of two-dimensional quasicrystal with twelvefold rotational symmetry. *Phys. Rev. Lett.* **60**, 1645–1648 (1988).
8. Hayashida, K., Dotera, T., Takano, A. & Matsushita, Y. Polymeric quasicrystal: Mesoscopic quasicrystalline tiling in ABC star polymers. *Phys. Rev. Lett.* **98**, 195502 (2007).

9. Zhang, J.W. & Bates, F.S. Dodecagonal Quasicrystalline Morphology in a Poly(styrene-b-isoprene-b-styrene-b-ethylene oxide) Tetrablock Terpolymer. *J. Am. Chem. Soc.* **134**, 7636-7639 (2012).

10. Gillard, T.M., Lee, S.W. & Bates, F.S., Dodecagonal quasicrystalline order in a diblock copolymer melt. *PNAS* **113**, 5167-5172 (2016).

11. Talapin, D.V., Shevchenko, E.V., Bodnarchuk, M.I., Ye, X.C., Chen, J. & Murray, C.B. Quasicrystalline order in self-assembled binary nanoparticle superlattices. *Nature* **461**, 964-967 (2009).

12. Xiao, C.H., Fujita, N., Miyasaka, K., Sakamoto, Y. & Terasaki, O. Dodecagonal tiling in mesoporous silica. *Nature* **487**, 349-353 (2012).

13. Urgel, J.I., Ecija, D., Lyu, G.Q., Zhang, R., Palma, C.A., Auwarter, W., Lin, N.A. & Barth, J.V. Quasicrystallinity expressed in two-dimensional coordination networks. *Nature Chemistry* **8**, 657-662 (2016).

14. Yue, K., Huang, M.J., Marson, R.L., He, J.L., Huang, J.H., Zhou, Z., Wang, J., Liu, C., Yan, X.S., Wu, K., Guo, Z.H., Liu, H., Zhang, W., Ni, P.H., Wesdemiotis, C., Zhang, W.B., Glotzer, S.C. & Cheng, S.Z.D. Geometry induced sequence of nanoscale Frank-Kasper and quasicrystal mesophases in giant surfactants. *PNAS* **113**, 14195-14200 (2016).

15. Passens, M., Caciuc, V., Atodiresei, N., Feuerbacher, M., Moors, M., Dunin-Borkowski, R.E., Blugel, S., Waser, R. & Karthauser, S. Interface-driven formation of a two-dimensional dodecagonal fullerene quasicrystal. *Nature Comm.* **8**, 15367 (2017).

16. Freedman, B., Bartal, G., Segev, M., Lifshitz, R., Christodoulides, D.N. & Fleischer, J.W. Wave and defect dynamics in nonlinear photonic quasicrystals. *Nature* **440**, 1166-1169 (2006).

17. Haji-Akbari, A., Engel, M., Keys, A.S., Zheng, X.Y., Petschek, R.G., Palffy-Muhoray, P. & Glotzer, S.C. Disordered, quasicrystalline and crystalline phases of densely packed tetrahedral. *Nature* **462**, 773-777 (2009).

18. Dotera, T., Oshiro, T. & Ziherl, P. Mosaic two-lengthscale quasicrystals. *Nature* **506**, 208-211 (2014).

19. Dotera, T., Bekku, S. & Ziherl, P. Bronze-mean hexagonal quasicrystal. *Nat. Mat.* **16**, 987 (2017).

20. Barkan, K., Diamant H. & Lifshitz, R. Stability of quasicrystals composed of soft isotropic particles. *Phys. Rev. B* **83**, 172201 (2011)

21. Ungar, G. & Zeng, X.B. Frank-Kasper, quasicrystalline and related phases in liquid crystals. *Soft Matter* **1**, 95-106 (2005).

22. Baake, M., Klitzing, R. & Schlottmann, M. *Physica A* **191**, 554 (1992).

23. Oxborrow, M. & Henley, C.L. Random square-triangle tilings: A model for twelvefold-symmetric quasicrystals. *Phys. Rev. B* **48**, 6966-6998 (1993).

24. Zhang, R.B., Zeng, X.B. & Ungar, G. Direct AFM observation of individual micelles, tile decorations and tiling Rules of a dodecagonal liquid quasicrystal. *J. Phys., Condens. Matter* **29**, 414022 (2017).

25. Wang, P.Y. & Mason, T. G. A Brownian quasi-crystal of pre-assembled colloidal Penrose tiles. *Nature* **561**, 94-99 (2018).

26. Dontabhaktuni, J., Ravnik, M. & Zumer, S. Quasicrystalline tilings with nematic colloidal platelets. *PNAS* **111**, 2464-2469 (2014).

27. Senyuk, B., Liu, Q., Bililign, E., Nystrom, P.D. & Smalyukh, I.I. Geometry-guided colloidal interactions and self-tiling of elastic dipoles formed by truncated pyramid particles in liquid crystals. Phys. Rev. E. **91**, 040501(R) (2015).

28. Reinhardt, A., Schreck, J.S., Romano, F. & Doye, J.P.K. Self-assembly of two-dimensional binary quasicrystals: a possible route to a DNA quasicrystal. *J. Phys. Condens. Matter* **29**, 014006 (2017).

29. Nova, E.G., Wong, C.K., Llombart, P. & Doye, J.P.K. How to design an icosahedral quasicrystal through directional bonding. *Nature* **596**, 367–371 (2021).

30. Ungar, G., Tschierske, C., Abetz, V., Holyst, R., Bates, M.A., Liu, F., Prehm, M., Kieffer, R., Zeng, X.B., Walker, M., Glettner, B. & Zywocinski, A. Self-Assembly at Different Length Scales: Polyphilic Star-Branched Liquid Crystals and Miktoarm Star Copolymers, *Adv. Funct. Mater.* **21**, 1296-1323 (2011).

31. Tschierske, C., Nürnberger, C., Ebert, H., Glettner, B., Prehm, M., Liu, F., Zeng X.B. & Ungar, G. Complex tiling patterns in liquid crystals, *Interface Focus* **2**, 669–680 (2012).

32. Chen, B., Zeng, X.B., Baumeister, U., Ungar, G. & Tschierske, C. Liquid crystalline networks composed of pentagonal, square, and triangular cylinders. *Science* **307**, 96-99 (2005).

33. Liu F., Chen B., Baumeister U., Zeng X.B., Ungar G. & Tschierske C. The triangular Cylinder Phase: A new Mode of Self-assembly in Liquid Crystalline Soft Matter, *J. Am. Chem. Soc.* **129**, 9578-9579 (2007),.

34. Chen B., Zeng, X.B., Baumeister, U., Diele, S., Ungar. G. & Tschierske C. Liquid Crystals with Complex Superstructures, *Angew. Chemie – Inter. Ed.* **116**, 4721-4725 (2004).

35. Ungar G., Liu F., Zeng X.B., Glettner B., Prehm M., Kieffer R. & Tschierske C. GISAXS in the study of supramolecular and hybrid liquid crystals, *J. Phys.: Conf. Ser.* **247**, 012032 (2010).

36. Liu F., Chen B., Glettner B., Prehm M., Das M. K., Baumeister U., Zeng X. B., Ungar G. & Tschierske C. The trapezoidal Cylinder Phase: A New Mode of Self-Assembly in Liquid-Crystalline Soft Matter, *J. Am. Chem. Soc.* **130**, 9666-9667 (2008).
37. Takakura H., Shiono M., Sato T. J., Yamamoto A. & Tsai A. P. Ab Initio Structure Determination of Icosahedral Zn-Mg-Ho Quasicrystals by Density Modification Method, *Phys. Rev. Lett.* **86**, 236–239 (2001).
38. Takakura H., Gómez C. P., Yamamoto A., de Boissieu M., Tsai A. P. Atomic structure of the binary icosahedral Yb-Cd quasicrystal, *Nat. Mater.* **6**, 58–63 (2007).
39. Gähler F. Crystallography of Dodecagonal Quasicrystals, pp. 272-284 in Quasicrystalline Materials, Janot C. & Dubois J.M. (eds.), World Scientific 1988.
40. Zeng X.B. & Ungar, G. Inflation rules of square-triangle tilings: from approximants to dodecagonal liquid quasicrystals. *Phil. Mag.* **86**, 1093-1103 (2006).
41. S. Förster, K. Meinel, R. Hammer, M. Trautmann & W. Widdra, Quasicrystalline structure formation in a classical crystalline thin-film system. *Nature* **502**, 215-218 (2013).
42. Lifshitz, R. & Diamant, H. Soft quasicrystals - Why are they stable? *Phils. Mag.* **87**, 3021-3030 (2007).
43. Poppe M., Chen C., Poppe S., Liu F. & Tschierske C. A periodic dodecagonal supertiling by self-assembly of star-shaped molecules in the liquid crystalline state, *Comms. Chem.* **3**, 70 (2020).
44. Engel M., Damasceno P. F., Phillips C. L. & Glotzer S. C. Computational self-assembly of a one-component icosahedral quasicrystal, *Nat. Mater.* **14**, 109–116 (2015).
45. Zeng, X.B., Kieffer, R., Glettner, B., Nurnberger, C., Liu, F., Pelz, K., Prehm, M., Baumeister, U., Hahn, H., Lang, H., Gehring, G.A., Weber, C.H.M., Hobbs, J.K. & Tschierske, C. Complex Multicolor Tilings and Critical Phenomena in Tetraphilic Liquid Crystals. *Science* **331**, 1302-1306 (2011).
46. Glettner, B., Liu, F., Zeng, X.B., Prehm, M., Baumeister, U., Walker, M., Bates, M.A., Boesecke, P., Ungar, G. & Tschierske, C. Liquid-Crystalline Kagome. *Angew. Chem. – Inter. Ed.* **47**, 9063-9066 (2008).
47. Liu, F., Kieffer, R., Zeng, X.B., Pelz, K., Prehm, M., Ungar, G. & Tschierske, C. Arrays of giant octagonal and square cylinders by liquid crystalline self-assembly of X-shaped polyphilic molecules, *Nat. Comm.* **3**, 1104 (2012).

Methods

Optical methods and DSC. Phase transitions were determined by polarizing microscopy (Leica DMR XP) in conjunction with a heating stage (FP 82 HT, Mettler) and controller (FP 90, Mettler) and by differential scanning calorimetry (DSC 8000, Perkin Elmer) at heating/cooling rates of 10 K min^{-1} (peak temperatures). If not otherwise noted transition temperatures and – enthalpies were taken from the second heating and cooling curve. Optical investigation was carried out under equilibrium conditions between glass slides which were used without further treatment, sample thickness was ~15 μm. A full wavelength retardation plate was used to determine the sign of birefringence. Optical micrographs were taken using a Leica MC120HD camera.

Powder X-ray scattering and aligned samples. Powder X-ray investigations were carried out with a Guinier film camera (Huber), samples in glass capillaries ($\varnothing$ 1 mm) in a temperature-controlled heating stage, quartz-monochromatized CuK$_\alpha$ radiation, 30 to 60 min exposure time, calibration with the powder pattern of Pb(NO$_3$)$_2$. Aligned samples were obtained on a glass plate. Alignment was achieved upon slow cooling (rate: 1 K·min^{-1} – 0.01 K·min^{-1}) of a small droplet of the sample and takes place at the sample–glass or at the sample–air interface, with domains fiber-like disordered around an axis perpendicular to the interface. The aligned samples were held on a temperature-controlled heating stage and the diffraction patterns were recorded with a 2D detector (HI-STAR, Siemens).

Synchrotron X-ray diffraction experiments. High-resolution small-angle powder diffraction experiments were recorded on Beamline I22 of the Diamond Light Source. Samples were held in evacuated 1 mm capillaries. A modified Linkam hot stage was used, with a hole for the capillary drilled through the silver heating block and mica windows attached to it on both sides. A 2D detector was used to record the diffraction pattern which is then converted by integration into 1D q-space. Q calibration and linearization were verified using several orders of layer reflections from silver behenate and a series of n-alkanes. To keep samples dry, the samples prepared in glass capillaries were vacuumed in melt and then sealed.

Grazing incidence X-ray diffraction (GIXRD) experiments were carried out on Beamline BM28, ESRF at Grenoble, and station BL40B2 at Spring-8, Japan. Thin film samples were prepared from melt on silicon substrates. The diffraction patterns were recorded on 2D CCD detectors. The thin film samples were placed on top of a heating stage for temperature control. To keep the samples dry, the samples were flushed with dry helium at BM28, and kept under vacuum at Spring-8, during the GIXRD.

Reconstruction of electron density maps. Fourier reconstruction of the electron density was carried out using the general formula for 2D periodic systems:

$$\rho(xy) \ = \ \sum_{hk} F(hk) \, exp[2\pi i(hx + ky)] \ = \ \sum_{hk} \sqrt{I(hk)} \, exp[2\pi i(hx + ky) + i\phi(hk)]$$

Specific formulae for the different plane groups can be found in International Tables of Crystallography.

Data availability

All data generated or analysed in this study are available in this article and its Supplementary Information. Source data are provided.